Photoconductivity and optical properties in composites of poly(paraphenylene vinylene) and single-walled carbon nanotubes

E. Mulazzi and R. Perego
Dipartimento di Fisica, Universitá degli Studi di Milano and Istituto Nazionale di Fisica della Materia, Via Celoria, 16, 20133 Milano, Italy

H. Aarab,* L. Mihut,† S. Lefrant, E. Faulques, and J. Wéry
Laboratoire de Physique Cristalline, Institut des Matériaux Jean Rouxel, 2 rue de la Houssinière, BP32229, F-44322 Nantes, France
(Received 6 September 2003; revised manuscript received 18 February 2004; published 29 October 2004)

We present photoconductivity and Raman scattering data obtained from composite films of poly(paraphenylene vinylene) (PPV) and single-walled carbon nanotubes at different weight concentrations from 0% to 64%. It is found that the introduction of nanotubes in the PPV precursor polymer solution, heated at 300 °C to perform conversion into PPV, yields drastic modifications in both the structural features of the composite components and in the electronic properties of the composites. The PPV polymer matrix becomes more disordered due to the introduction of nanotubes which induce a shortening of the polymer conjugated segments as shown by Raman scattering spectra. In addition, these spectra yield information about the evolution from small bundles to thick bundles of single-walled nanotubes as function of their concentration x. Photoconductivity data show that the percolation regime begins at $x=2\%$, indicating that a migration network for the photogenerated charges is established above this threshold. By using a model based on distributions of PPV conjugated lengths and their changes as function of x, we calculate the Raman scattering band shapes and their relative intensities. The theoretical results lead to a comprehensive interpretation of experimental data.

DOI: 10.1103/PhysRevB.70.155206 PACS number(s): 78.40.Ri, 78.55.Kz, 78.66.Qn, 78.66.Sq

I. INTRODUCTION

Conjugated polymers such as poly(paraphenylene vinylene) (PPV) and its derivatives can form with carbon nanotube composite films which are very promising materials for potential applications such as transport layers, or to be included in electronic devices, such as light emitting diodes (LED), for example. To this respect it seems very important to study the nature of photoexcitations in these systems. It has been reported previously[1–4] that the introduction of multiwalled (MWNT's) or single-walled carbon nanotubes (SWNT's) in polymer matrices modifies drastically both electrical and optical properties of the as-obtained composites. In particular, in such composites made with poly(*m*-phenylene vinylene-co-2,5-dioctoxy-*p*-phenylene vinylene) (PmPV), poly(3-octyl thiophene), and poly(methyl methacrylate) (PMMA) the electrical conductivity increases up to ten orders of magnitude. In photovoltaic devices based on ITO/PPV/MWNTs/Al (ITO stands for indium tin oxide), the external quantum efficiency of these compounds is twice that of ITO/PPV/Al.[5] Also, it has that been shown that photoluminescence (PL) of composite films is dramatically quenched and overall shifted towards the blue range of the optical spectrum as function of the MWNT's concentration.[1] Additionally, previous works have reported strong modifications of the PL spectrum in PPV thermally converted at 210 °C onto a MWNT layer.[6] These data are characteristics of interactions between PPV and carbon nanotubes. This was also reported recently in PPV derivatives/carbon nanotubes or C_{60} composites.[7]

Previously, we presented a detailed and comprehensive experimental and theoretical study of optical absorption and PL spectra of PPV/SWNT composite films at different concentrations from 0% to 64% obtained from precursor solutions thermally converted at 300 °C. We showed that the blue shift and the decrease in absorption intensity as well as the changes of the PL spectra are due to a shortening of the effective conjugation length in PPV chains due to the increase of the SWNT concentration in the polymer matrix. This result has been completely confirmed by a theoretical model for the absorption and the emission calculated bands.[8] Furthermore, the quenching of the PL intensity observed when the concentration x rises (from 0% to 64%) can be determined by the increase of short conjugation length segments in the film and by improved charge transfer from polymer segments to SWNT's.

In this paper, we present experimental and theoretical photoconductivity and Raman studies of PPV/SWNT composites to complete our previous works carried out in absorption and photoluminescence[8] in similar samples. Additional structural information are provided by means of transmission electron microscopy (TEM), scanning electron microscopy (SEM), and x-ray diffraction (XRD), together with Raman scattering. In particular, Raman scattering performed in the low-frequency region, via the radial breathing modes of nanotubes, is powerful to determine both their tube diameters and aggregation in bundles, whenever the tube concentration is sufficiently high. Otherwise, spectra recorded in the 1000–1700 cm^{-1} region exhibit features of both PPV conjugated chains and the so-called "G" mode of SWNT's. This mode is observed in carbon nanotubes, the origin of which being the E_{2g_2} mode of graphite. Therefore, on the one hand calculations of intensity ratios of Raman bands of PPV permit to test the distribution of chain conjugation lengths found

from the calculated absorption bands for the same samples. On the other hand, the evolution from small SWNT bundles to thick ones can be followed from the G band behavior.[9]

II. EXPERIMENTAL DETAILS

The sulfonium polyelectrolyte precursor polymer of PPV was synthesized in our laboratory via the standard procedure using the tetrahydrothiophenium group described elsewhere.[10] The powder of single-walled carbon nanotubes used in this study is produced by laser ablation.[11] The powder of SWNT's is dispersed in the methanol solution of the soluble precursor polymer with sonication at different weight concentrations of SWNT's. Note that this dispersion is quite uniform and stable without any nanotubes deposition for a period of several months. Thin films of these resulting mixtures were obtained by depositing the solution under a nitrogen flow onto silica substrates for optical absorption, Raman scattering, and onto silicon [100] single crystals or glass substrates for XRD measurements or SEM observations. Beforehand, all substrates were cleaned in an ultrasonic bath with deionized water and ethanol. Then thin films were subsequently heated under dynamic secondary vacuum at a typical temperature of 300 °C for about 6 h to achieve the conversion of the polymer precursor into PPV. The thickness of the obtained films is about 200 nm. Raman spectra have been recorded with different laser lines in the visible range (λ_L = 676.4 nm), in the near UV (λ_L = 363.8 nm), and in the near-infrared region (λ_L = 1064 nm), using a multichannel Jobin-Yvon T 64000 spectrometer equipped with a cooled detector and a Fourier-transform–Raman BRUCKER RFS 100 apparatus, respectively. The scattered signal was collected either at 90° or in backscattering geometries under microscope or in macroscopic configuration. The wave number resolution of the Raman spectra was 2 cm^{-1} in the near-IR and the visible region and 4 cm^{-1} in the near UV region. All measurements were carried out at room temperature and in ambient air. SEM images of the PPV/SWNT composite films were obtained by using a JEOL JSM 6400F microscope and high-resolution transmission electron microscopy (HRTEM) images by using a HITACHI HNAR 9000 microscope. In this latter case, the mixed solution of PPV precursor polymer/SWNT's is deposited by drop casting onto the Cu support grid in order to form thin free standing films (thickness about 40 nm). The films obtained were introduced into the electron microscope, then were heated *in situ* at 300 °C by means of a sample heater holder. Photoconductivity measurements were performed using the 488 nm line of an argon laser. Surface gold strips with a 1 mm interelectrode spacing are evaporated and contacted to the external circuit with an Ag-loaded epoxy resin and films are attached to the cold finger of a cryostat. A high sensitivity (10^{-15} A) Keithley digital electrometer model 6517 was used to detect the observed photocurrent. The ohmic law was checked up to 300 V/cm and the data were recorded by using a field of 100 V/cm. The dark current increased drastically by 11 orders of magnitude from x = 0% to 32%.

III. RESULTS

SEM images of PPV/SWNT composite films at different concentrations x show that at high SWNT's concentration, the porosity of the composites increases with a dense nanotubes network. For x = 16%, individual separated bundles are well observed while for x = 64% SWNT's are mixed in the polymer network. Details will be published elsewhere.[12] In Fig. 1, we show the HRTEM image of the sample at x = 64% where we can see three bundles of about 20 nm in width. Each bundle consists of about 15 SWNT's whose individual diameter is around 1.33 nm. Let us note that in this micrograph, one observes also a metallic particle encapsulated in amorphous carbon. From a preliminary and comparative analysis of the x-ray diagrams of PPV and PPV/SWNT composite films, one can deduce that structural disorder and inhomogeneity rise in the polymer matrix of the composite by increasing the concentration of nanotubes.[13,14] This implies a decrease of the coherence length in the polymer component.

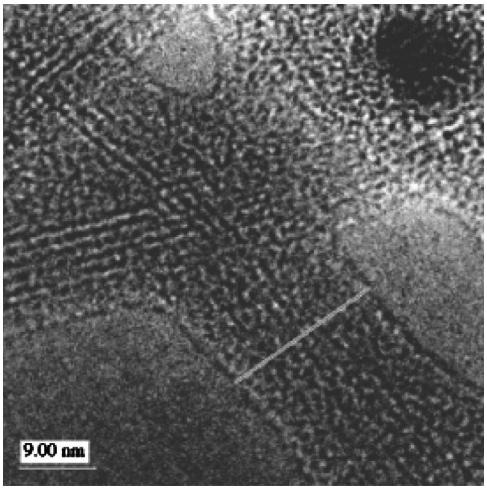

FIG. 1. High-resolution transmission electron microscopy image for the composite film at x = 64%.

In Fig. 2 we present the photoconductivity data taken for an excitation λ_L = 488 nm. In our experiment the percolation

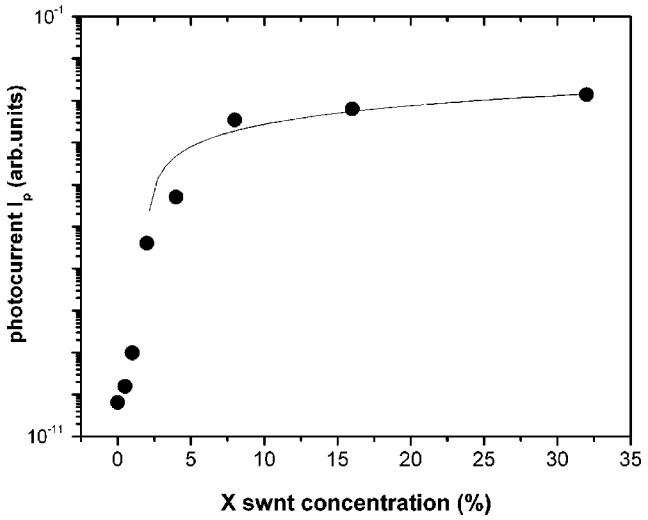

FIG. 2. Photocurrent at room temperature as function of weight percentages x for the excitation λ_L = 488 nm. The solid line is a fit to the data using the percolation model.

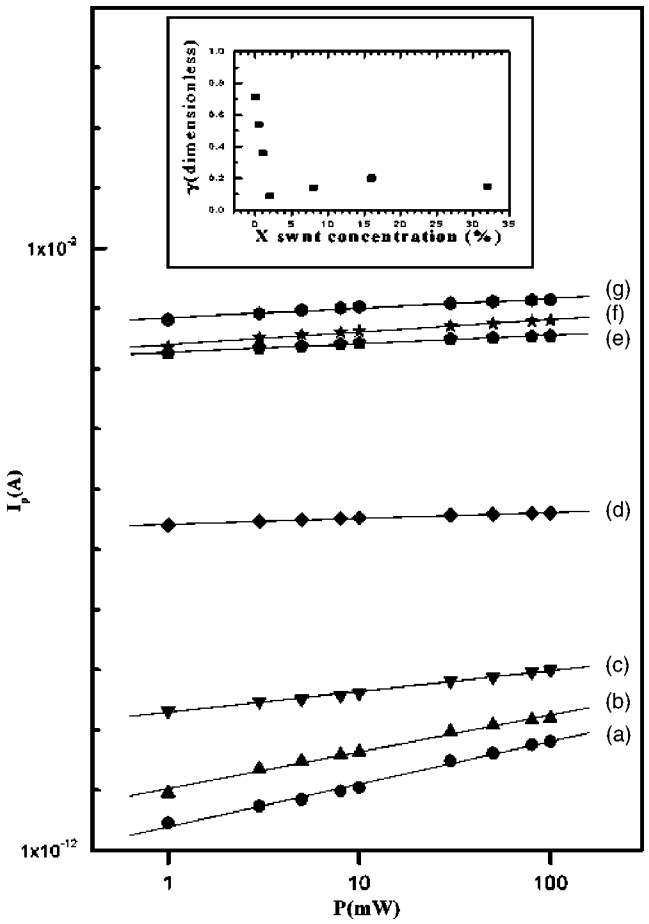

FIG. 3. Light power P dependence of the photocurrent I_p at room temperature for standard PPV and PPV-SWNT composites films for different SWNT weight percentages x. (a) standard PPV, (b) $x=0.5\%$, (c) $x=1\%$, (d) $x=2\%$, (e) $x=8\%$, (f) $x=16\%$ and (g) $x=32\%$. Inset shows the variation of exponent γ versus x. Abscissa and ordinate axes are given in decimal logarithmic scales.

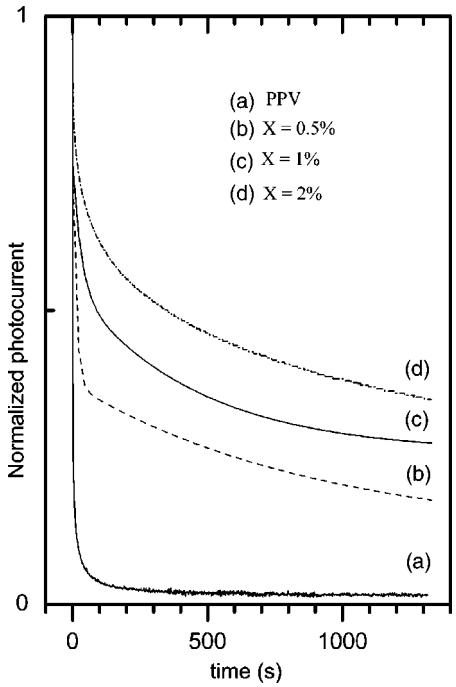

FIG. 4. Decay of the normalized photocurrent for the standard PPV and PPV-SWNT composites films for different SWNT weight percentages x. (a) standard PPV, (b) $x=0.5\%$, (c) $x=1\%$, and (d) $x=2\%$.

regime begins at $x=2\%$ and is characteristic of a three-dimensional system. The data given in Fig. 2 have been fitted using a percolation model[15] from which the percolation regime threshold and the dimensionality of the systems can be derived. In the system we have considered here, the dimensionality parameter is found to be $\beta=2$ for the photoconductivity. Note that the values of photoconductivity change by seven orders of magnitude in the range from 0% to 8%, after which a "plateau-type" curve is reached.

The light power dependence P of the photocurrent I_p was studied for each composite sample (from $x=0\%$ to 32%) by varying the light intensity with neutral density filters (Fig. 3). A power-law dependence $I_p \propto P^{\gamma}$ is found for all x and the variation of γ versus x is shown in the inset of Fig. 3. The minimum of this curve is found around $x=2\%$, which is the threshold of the percolation regime, in agreement with the value found previously. This curve, in addition, is characteristic of two different regimes. When $x<2\%$, γ decreases from 0.75 to 0.20 as a signature of the introduction of a larger state of disorder, decreasing the recombination mechanism. When $x>2\%$, γ is stabilized at 0.20, the system being presumably dominated by a dissociation of the excitons, and migration of charge carriers. In a concomitant way, this result is in agreement with the PL quenching reported in Ref. 8 for high x concentrations. This point can be further argumented by measurements of lifetime of the photocurrent below the percolation threshold ($x<2\%$). In Fig. 4 we present the normalized photocurrent for different composite samples after the laser excitation has been switched off at $t=0$, and for the same pump power. The lifetime of the photocarriers increases substantially when x increases, in agreement with the large state of disorder introduced above. In the second regime ($x>2\%$), the photocarriers are trapped more easily on PPV segments, since the nanotubes favor charge transport and the lifetime is shorter.

In Fig. 5 we show the maximum of photocurrent for $x=2\%$ as function of temperature in semilogarithmic scale. The photocurrent is decreasing with decreasing temperature due to the lower mobility of the photocharges and the increasing probability to be trapped. Due to this effect the intensity of the PL increases at lower temperature in PPV samples as shown in Ref. 16. The photocurrent is thermally activated with an activation energy of 0.20 eV. This value is very near the thermal activation value of pristine PPV (0.25 eV).[17] This result implies that photoconductivity is due to PPV photogenerated charges and the SWNT fraction in the composite provides only the migration network for the charges. The state of disorder that is invoked above to explain the behavior of the photoconductivity data can be checked by additional spectroscopic measurements. In particular, Raman scattering performed on PPV has been shown to be a powerful tool to check the effective length of conjugated segments by a determination of distributions of chain lengths in various samples.[18]

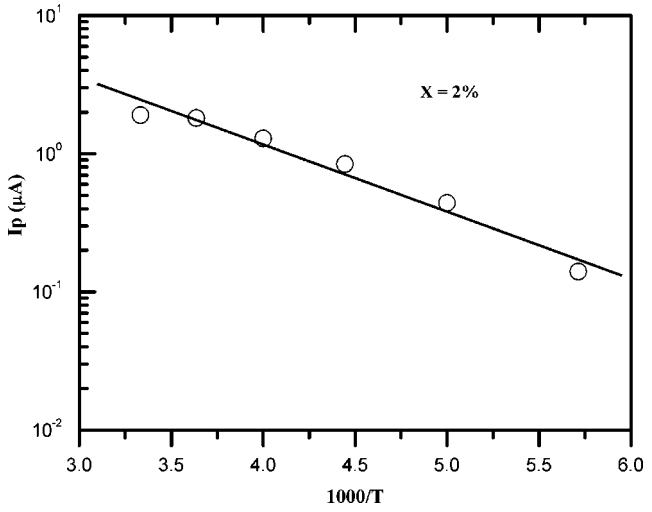

FIG. 5. Maximum photocurrent of the $x=2\%$ composite versus temperature. The solid line is a linear fit with the Arrhenius law. The ordinate axis is in decimal logarithmic scale.

In Fig. 6, Raman scattering spectra in the range 120–220 cm^{-1} are displayed as function of the SWNT concentration x in the composite films. The evolution of the breathing mode band [Figs. 6(a)–6(g)] observed in the range 160–180 cm^{-1} in the composite films is presented for $\lambda_L = 1064$ nm. The band at 160 cm^{-1} [Fig. 6(b)] progressively decreases when x increases, while another peak around 180 cm^{-1} concomitantly grows in intensity reaching a maximum in Fig. 6(g) for $x=64\%$. This result can be explained by the aggregation of SWNT's from isolated tubes to small bundles and to thick ones.[19] In fact, the frequency of the breathing mode in this frequency region is modified by the van der Waals interaction between isolated nanotubes,[20–22] and the strength of this interaction increases as function of x. Using excitation wavelengths in the red range for which the Raman response of metallic tubes is resonantly enhanced, i.e. 676.4 nm, a similar global behavior is found, in particular for concentrations of nanotubes higher than 8%. Again our results are in rather good agreement with those presented in Ref. 19, showing combined Raman and x-ray data of thin bundles and thick bundles of nanotubes, respectively.

We present in Fig. 7 Raman spectra taken with $\lambda_L = 676.4$ nm of composite films for different concentrations of nanotubes in the range 1100–1700 cm^{-1}. We compare to the spectrum of pristine PPV which exhibits the standard features, i.e., five main bands at 1174, 1340, 1550, 1586, and 1625 cm^{-1}, the assignment of which being published previously[23] (see Table I). Let us recall that a complete study was consequently carried out[18] showing that the stretching vibrations of the vinyl group and the phenyl ring do not significantly change in frequency with laser excitation wavelength, since only an upshift of a few wavenumbers is recorded when higher excitation energies are used. An important feature, however, concerns the intensity ratio between the 1550 and 1625 cm^{-1} Raman bands. Due to resonance conditions with the electronic transitions of long conjugated segments, this ratio is larger than one for $\lambda_L = 676.4$ nm, as it is shown in Ref. 18. As x increases the main features of the

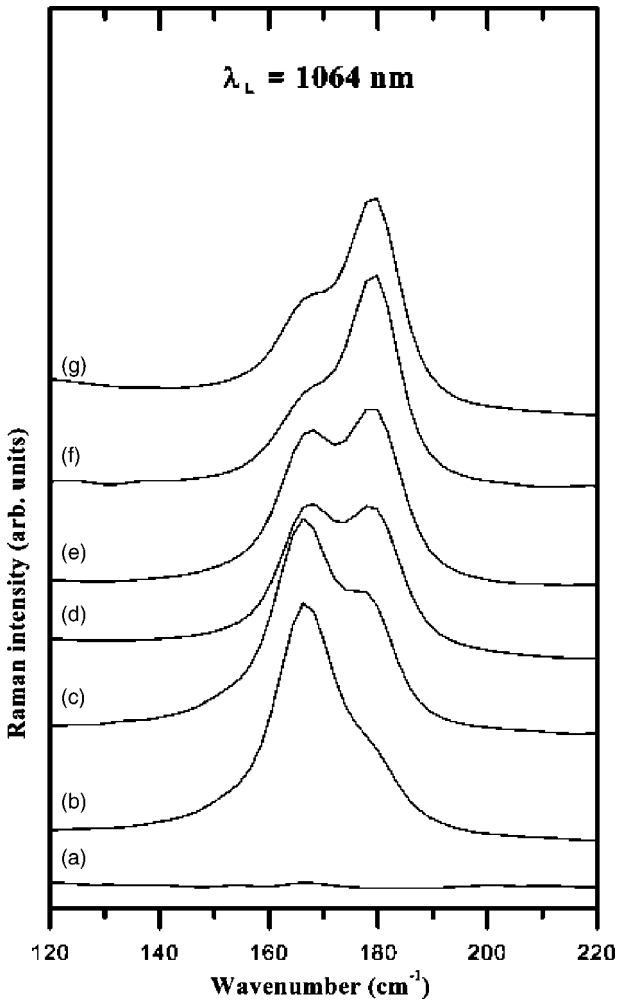

FIG. 6. Raman scattering spectra of the composite films at room temperature taken with $\lambda_L = 1064$ nm in the frequency region 120–220 cm^{-1}. (a) $x=0$, (b) $x=1\%$, (c) $x=2\%$, (d) $x=8\%$, (e) $x=16\%$, (f) $x=32\%$, and (g) $x=64\%$.

spectra are determined by the nanotubes vibrations contributing to the band at 1300 cm^{-1} (D band) which has been ascribed to intrinsic defects and disordered graphitic structures. Moreover, for this excitation wavelength, at high SWNT's concentrations, the Breit-Wigner-Fano component of metallic tubes (G band) is obviously recorded and this part of the spectrum resembles that of pristine SWNT's as shown in Fig. 7(g).[24] Notice that this is consistent with the formation of thick bundles embedded in the polymer matrix. On the other hand concerning the PPV polymer, we note that the intensity of the Raman band at 1174 cm^{-1} is decreasing as x increases. This effect is due to the increase of the short segments in the sample and to the decrease of the relative contribution of PPV segments to the Raman scattering.[18]

In Fig. 8 we show the resonant Raman spectra with the excitation wavelength $\lambda_L = 363.8$ nm of PPV and PPV/SWNT composite films at different concentrations. In this figure we observe only the contributions to the Raman scattering coming from the vibrations of PPV segments, since only the electronic transitions of these segments are in resonance with this excitation wavelength, with no contribution

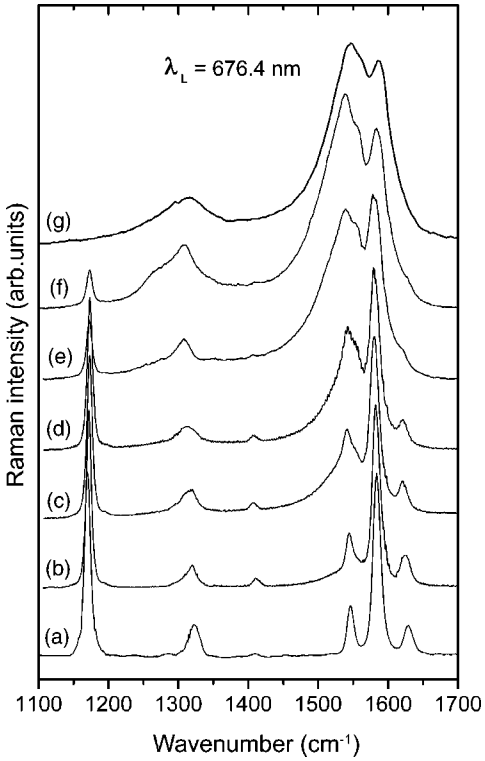

FIG. 7. Raman scattering spectra of the composite films at room temperature for $\lambda_L = 676.4$ nm in the range 1100–1700 cm^{-1}. (a) $x=0$, (b) $x=1\%$, (c) $x=2\%$, (d) $x=8\%$, (e) $x=32\%$, (f) $x=64\%$, and (g) SWNT powder.

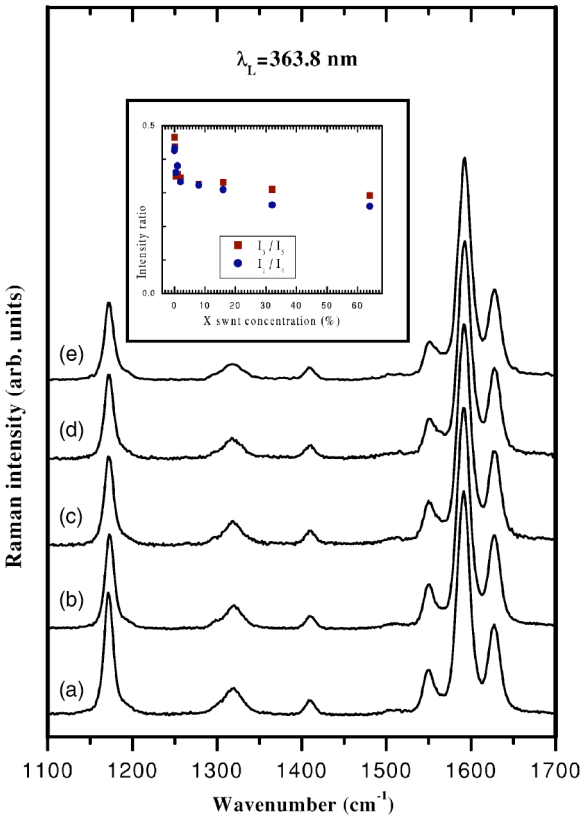

FIG. 8. Resonant Raman scattering spectra of the composite films at room temperature for $\lambda_L = 363.8$ nm. (a) $x=0$, (b) $x=2\%$, (c) $x=8\%$, (d) $x=32\%$, and (e) $x=64\%$. In the inset we show the intensity ratios I_3/I_5 and I_1/I_4 as a function of x.

of SWNT's. The spectrum is characterized by five main bands at almost the same frequency as given before in Table I. From Fig. 8 we can notice that the intensity ratios $I(1174)/I(1586)$ (I_1/I_4) and $I(1551)/I(1627)$ (I_3/I_5) decrease as x increases from 0% to 64% (see inset of Fig. 8). This trend is a signature in the different samples of an increase of the short segment percentage with respect to that of the long segments.[18] In addition, this behavior is equivalent to that observed from partially PPV converted samples at different temperatures.[25]

In the spectra shown in Fig. 8 there is an additional feature at 1411 cm^{-1} already observed in Fig. 7. This feature is more intense for $\lambda_L = 363.8$ nm and its relative intensity increases with x. This small band is again a signature of a partial conversion of the prepolymer solution as observed in spectra taken at different conversion temperatures for pristine PPV,[25] in which it is shown that it increases when the conversion temperature decreases. This band is ascribed to a vibration of the precursor polymer which turns out to be Raman and infrared active, presumably as a consequence of an increased disorder in the samples.

TABLE I. Assignments of the most intense Raman active modes of PPV.

f	Frequency ω_f (cm^{-1})	Main assignment
1	1174	C—C stretching + C-H bending of the phenyl ring
2	1330	C═C stretching + C-H bending of the vinyl ring
3	1550	C═C stretching of the phenyl ring
4	1586	C—C stretching of the phenyl ring
5	1625	C═C stretching of the vinyl group

In order to interpret the Raman scattering data, we have carried out calculations on the model published previously[18] in both resonance and preresonance (RRS) conditions for PPV. To do so, we use the functions $\alpha_f(\Omega_L, \omega)$ of the first-order RRS cross sections[18] for each vibrational frequency ω_f considered, given in the following equation:

$$\alpha_f(\Omega_L,\omega) \approx \sum_{n=2}^{10} |M_n|^4 S_{f,n} \left| \sum_{l=0}^{1} (-)^l R_n(\Omega_L - l\omega_f) \right|^2 \times \frac{1}{\sqrt{2\pi}\Delta_f} \exp\left[-\left(\frac{\omega - \omega_f}{2\Delta_f} \right)^2 \right] P_n, \quad (1)$$

where Ω_L is the laser excitation frequency, ω is the frequency in the Stockes range, Δ_f is the width of the Raman band considered whose maximum is at ω_f given in Table I, and M_n is the electric dipole moment intensity for the electric transition to the $1B_u$ state of each oligomer with n phenyl rings,[26] whose frequency is indicated by Ω_n (see Table II). The functions $R_n(\Omega_L - l\omega_f)$ for $l=0$, 1 which weight for each

TABLE II. Values of Ω_n, $S_{f,n}$, and γ_n, used for the calculated Raman scattering band shapes and the intensity ratios of different PPV and PPV-SWNT samples.

n	2	3	4	5	6	7–10
Ω_n(eV)	3.78	3.25	3.00	2.86	2.75	2.60
$S_{1,n}$	0.40	0.40	0.42	0.45	0.50	0.52
$S_{2,n}$	0.10	0.08	0.08	0.08	0.08	0.08
$S_{3,n}$	0.12	0.12	0.12	0.15	0.20	0.20
$S_{4,n}$	0.96	0.95	0.92	0.92	0.75	0.70
$S_{5,n}$	0.32	0.25	0.23	0.15	0.15	0.10
γ_n(eV)	0.12	0.12	0.14	0.16	0.18	0.20

oligomer of length n the cross section, are given in the following equation:

$$R_n(\Omega_L) = \exp\left[-\sum_{f=1}^{5} S_{f,n}\right]\sum_{j=0}^{2}\sum_{f=1}^{5}\frac{(S_{f,n})^j}{(j)!} \times \frac{\gamma_n + i(\Omega_L - \Omega_n - j\omega_f)}{\gamma_n^2 + (\Omega_L - \Omega_n - j\omega_f)^2}. \quad (2)$$

In Eq. (2), $S_{f,n}$ are the contributions to the total Huang-Rhys factors $S_n = \Sigma_{f=1}^{5} S_{f,n}$ which come from each vibrational mode (labeled by f) interacting with the electronic excited state $1B_u$ of every oligomer with n phenyl rings. These contributions are related to the electron-vibrational couplings for each vibrational stretching mode we consider here ($f=1-5$) and whose frequency is indicated by ω_f. $j=0$, 1, 2 numbers the vibronic processes considered in the following calculations (up to two vibronic processes) in the same approximation as we have used in the optical absorption calculation.[8,18] In this paper, we do not take into account any change of ω_f with n, which is related to the length of the segments.

In Table II, we give Ω_n, $S_{f,n}$ and the damping factors γ_n, for $T=300$ K. Ω_n have been evaluated in the same approximation as in Ref. 27, and they are in agreement with the data reported there. $S_{f,n}$ are fitted from the Raman experimental spectra of the oligomers, taking into account also the properties of the electron vibrational couplings in the $1B_u$ excited states for intermediate and short segments.[28] As it can be seen from Table II, $S_{f,n}$ change as function of the stretching mode frequencies ω_f ($f=1-5$) and of the number of the phenyl rings n. In particular, $S_{1,n}$ and $S_{3,n}$ increase for n going from 2 to 10, while $S_{4,n}$ and $S_{5,n}$ decrease and $S_{2,n}$ do not show a significant change in the same range of n. This is due to the different behavior of the five electron vibrational couplings coming from the decreasing localization of the electronic states $1B_u$ for increasing n.

We want to note that all the values given in Table II and which are used in the calculated RRS spectra given in the following are the same than those used for the optical absorption calculation from the same samples.[8] In Eq. (1) we have weighted the contributions of the ω_f coming from the effective lenghts with n phenyl rings with P_n, the double Gaussian distribution given in Eq. (3).

TABLE III. Distribution parameters used in the calculations of the Raman scattering band shapes and the intensity ratios of standard PPV and PPV-SWNT composite films for different weight percentages x from 0.5% to 64%. Standard PPV is indicated with $x=0$.

x	n_1	σ_1	n_2	σ_2	G
0	3	1	8	2	0.3
0.5	3	1	7	2	0.26
1	2	1	6	1	0.2
2	2	1	5	1.4	0.3
16	2	1	5	1.2	0.29
32	2	1	5	0.9	0.22
64	2	1	5	0.7	0.21

$$P_n = \frac{1-G}{(2\pi\sigma_1)^{1/2}}\exp\left[-\left(\frac{n-n_1}{\sqrt{2}\sigma_1}\right)^2\right] + \frac{G}{(2\pi\sigma_2)^{1/2}} \times \exp\left[-\left(\frac{n-n_2}{\sqrt{2}\sigma_2}\right)^2\right], \quad (3)$$

where n_1 and σ_1 are the values of the most probable segment lengths and the related dispersion, respectively, of the distribution for $n=2-6$ (short oligomers), while n_2 and σ_2 are the values for the parameters related to the distribution for $n=7-10$ (intermediate length oligomers). G is the weight of the second distribution with respect to the first one. All the distribution parameters used in the calculated RRS spectra are given Table III. We note that these are the same as those used in calculated absorption spectra given in Ref. 8. In all the calculated spectra shown in the following, Δ_f, appearing in Eq. (1), is equal to 7 cm^{-1} and is constant for all f.

In Figs. 9(a) and 9(b) we show the calculated spectrum for $\lambda_L=676.4$ nm and 363.8 nm for the sample $x=2\%$ by using the values given in Tables I–III. The relative intensities of the main peaks are in very good agreement with those shown in Fig. 7(a). The calculated changes of the intensity

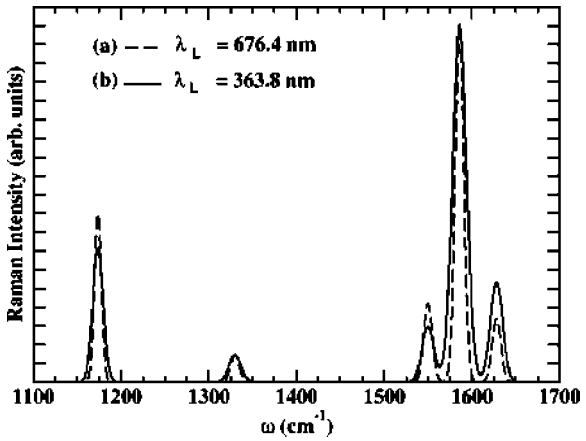

FIG. 9. Calculated Raman scattering spectra in preresonance ($\lambda_L=676.4$ nm) and resonance conditions ($\lambda_L=363.8$ nm) at RT of the composite films with $x=2\%$. (a) $\lambda_L=676.4$ nm, (b) $\lambda_L=363.8$ nm.

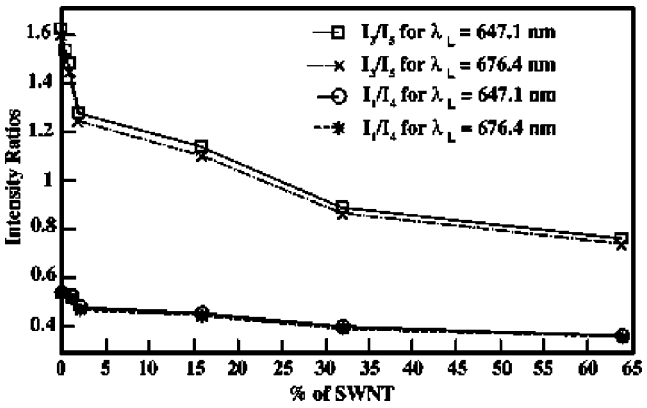

FIG. 10. Calculated intensity ratios I_3/I_5 and I_1/I_4 as function of x (percentage of SWNT weight) for $\lambda_L=647.1$ and 676.4 nm.

ratio of $I(1174)/I(1586)=I_1/I_4$ and $I(1550)/I(1625)=I_3/I_5$ as function of x concentrations are shown in Fig. 10 for $\lambda_L=676.4$ nm and $\lambda_L=647.1$ nm. From these data one can derive that the calculated ratio I_1/I_4 shows a decrease of I_1, the peak intensity at 1174 cm^{-1}, when x increases, as experimentally observed. We note that in these calculated ratios, we do not take into account the decrease of the PPV fraction in the composites as x increases, which is responsible of a further decrease in the experimental data.

In Fig. 11(a) the calculated spectrum for the $x=64\%$ sample is shown for $\lambda_L=363.8$ nm. In Fig. 11(b) the changes of the intensity ratios I_1/I_4 and I_3/I_5 versus x concentrations

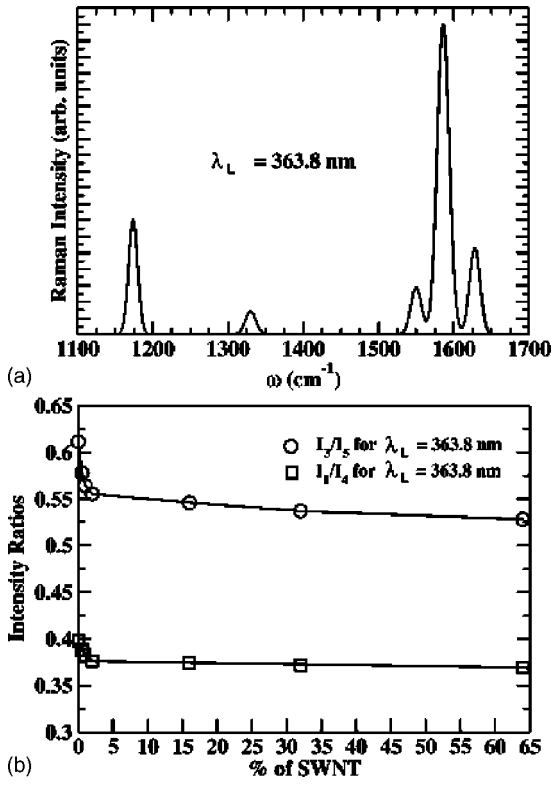

FIG. 11. (a) Calculated resonant Raman scattering at RT of the composite films at $x=64\%$ for $\lambda_L=363.8$ nm; (b) calculated intensity ratios I_3/I_5 and I_1/I_4 as function of x (percentage of SWNT weight) for $\lambda_L=363.8$ nm.

are shown. All the results shown in Figs. 9(b), 11(a), and 11(b) are in excellent agreement with experimental data of Fig. 8.

IV. DISCUSSION

In this paper we have presented several experimental data of PPV/SWNT composites, by using different techniques: TEM, photoconductivity, and Raman scattering. Our aim is to reach a more comprehensive understanding of the effects of nanotube introduction in the polymer precursor of PPV subsequently heated at 300 °C. This study should complete a previous investigation presented in Ref. 8 about experimental and calculated absorption and PL spectra of the same samples.

From XRD studies carried on our composites as a function of the SWNT concentration we observed an average decrease of the coherence length of the PPV polymer, as an indication that the structural order of the polymer matrix is affected by the presence of nanotubes, leading to a more amorphous compound. In parallel way, the presence of bundles of nanotubes is demonstrated.[29] From similar data reported on standard PPV and on samples prepared at different temperatures,[14] we can deduce that the presence of nanotubes in the polymer precursor prevents a complete thermal conversion of this precursor into PPV. The increase of the SWNT concentration leads to a system which behaves like a PPV sample converted at a lower temperature. It is known that this decrease is responsible for obtaining PPV samples characterized by shorter effective conjugation lengths.[25]

These results are furthermore corroborated by experimental Raman scattering results. In addition, calculations of the relative intensity of the Raman bands of PPV segments demonstrate changes as a function of λ_L and x, as a proof of the shortening of the effective conjugation lengths. This result brings to the same conclusion as proposed in Ref. 8 where the optical absorption and the PL emission together with the calculated spectra have been reported as a function of x. In fact, we have proved there that all the variations of the optical absorption spectra as function of x are the signatures of the fact that the polymer precursor is not totally converted. The main changes are the blue shift of the $\pi \rightarrow \pi^*$ main band, the shift and the intensity increase of the bands initially (for $x=0$) at 4.7 eV and the intensity rise of the peak at 6 eV. All these modifications in the spectra, as proposed in Ref. 8, can be related to the shortening of PPV conjugation lengths and to the tetrahydrothiophenium group contribution.

Furthermore, with the Raman data on SWNT's, in the range 1450–1650 cm^{-1} for $\lambda_L=676.4$ nm (see Fig. 7), we have proved that as function of x, the SWNT bundles change from small (see for instance $x=16\%$) to thick bundles ($x=64\%$). The change of the band shape in this frequency region is due to the Fano coupling which becomes more effective in thick bundles as reported in Ref. 19. In our experiment, the evolution of the band shape as a function of x is very well demonstrated. These results are also confirmed by the Raman scattering data in the range 120–220 cm^{-1} for the same wavelength.

The change of the RBM mode frequency from about 160 cm^{-1} to about 180 cm^{-1} as a function of x is due to the

evolution from isolated tubes or small bundles into thick bundles. This is an effect of van der Waals interaction between tubes[30] and/or an effect of the pressure induced on the bundles by the PPV polymer.[31] All these data are in excellent agreement with those obtained with TEM shown in Fig. 1, where for $x=64\%$ the packaging of bundles is very well observed.

In this paper we have also presented data of PC as function of the SWNT concentration x. Let us recall the previous conductivity measurements on PmPV-SWNT composites given in Ref. 2 show a percolation behavior with a threshold of approximately 8.5% nanotubes mass fraction. It is pointed out that two regimes of current versus voltage are recorded for low and high fields.[2] In our case, beginning from $x=2\%$ we observe the dramatic increase of the PC which shows a percolation behavior. This can be interpreted by the fact that a low fraction of SWNT's is sufficient to create a network for the migration of the charge carriers. Therefore, SWNT's are responsible for both effects: the shortening of the PPV segments during its conversion and the migration network of charge carriers. The data of PC are in very good agreement with the interpretation we have proposed for the PL data. Indeed, we showed that the intensity of PL spectra is dramatically quenched for the composite films with increasing x.[8] This effect can be interpreted by considering the decrease of the PPV fraction in composite films for different x and the increase of the PC, as we report in the present paper. Moreover, we have shown in Ref. 8 that PL spectra taken from composite films with different x are characterized by important changes in the emission band shapes. All the changes in the PL bandshape are very well reproduced by a model based on the interchain and intrachain dynamics of the excitations and on shortening of the effective conjugation lengths. Then, the PL only occurs if the excitations remain trapped on short segments or migrate on longer segments of PPV without encountering the SWNT network. On the other hand, the migration network of SWNT's prevents the radiative recombination of charges and increases the probability of charge separation and therefore of the PC. This type of charge transfer has been reported previously.[4,32,33] As a final remark, our method of preparation of PPV/SWNT composites leads to a system in which the percolation threshold is very low (2%). This behavior is consistent with the PL and PC mechanisms as discussed in the present paper. This may be surprising in view of previously reported results[2], although not unique in polymer-nanotube composites. Our method of preparation implies the mixing of the precursor polymer and nanotubes dispersed in methanol. In that case, a strong interaction between the two components may arise, the precursor polymer acting like a surfactant and therefore dispersing the nanotubes. The low percolation behavior can then result from the shape of the tubes which provide easily the migration network mentioned above. In a concomittant way, the interaction can prevent the total conversion of the precursor polymer into PPV upon thermal annealing. This last effect is then responsible for the shortening of the conjugation length of PPV, as demonstrated by our experimental and theoretical results obtained in both absorption, photoluminescence, and Raman scattering. Then the 2% threshold of the percolation behavior of the PC data turns out to be also important to put in evidence the consequences of the conjugation length shortening in all optical data of the PPV component in the composite films, as discussed above.

V. CONCLUSION

In conclusion, we have presented in this paper photoconductivity and Raman scattering data obtained on PPV/SWNT composites, in which the concentration of nanotubes has been varied from 0% to 64% in weight. Our results complete those previously published, reporting results in UV-visible absorption and photoluminescence. The theoretical analysis leads to a coherent interpretation in terms of segment length distributions in the PPV polymer. In particular, a shortening of the conjugation length of PPV explains the obtained experimental data, such as the behavior of the photoluminescence occurring if charge carriers remain trapped on short segments or migrate on longer segments without encountering the SWNT network. In this respect, the PC data are very important to explain the decrease of the photoluminescence intensity, as discussed in the text.

ACKNOWLEDGMENTS

The authors thank R. Almairac for experimental help in x-ray diffraction. The participation of A. M. Marie and C. Godon in the TEM experiments is greatly acknowledged. The Institut des Matériaux Jean Rouxel is Unité Mixte de Recherche au CNRS-Université de Nantes No. 6502.

*Permanent address: Laboratoire de Physique du Solide, Faculté des Sciences Dhar mehraz, B.P. 1796, Fès, Morocco.

†Permanent address: National Institute of Materials Physics, Lab 160, Bucharest, P.O. Box MG-7, 76900, Romania.

[1] S. Curran, P. M. Ajayan, W. J. Blau, D. L. Carroll, J. N. Coleman, A. B. Dalton, A. P. Davey, A. Drury, B. McCarthy, S. Maier, and A. Stevens, Adv. Mater. (Weinheim, Ger.) **10**, 1091 (1998).

[2] J. N. Coleman, S. Curran, A. B. Dalton, A. P. Davey, B. McCarthy, W. Blau, and R. C. Barklie, Phys. Rev. B **58**, R7492 (1998).

[3] J. M. Benoit, B. Corraze, S. Lefrant, W. J. Blau, P. Bernier, and O. Chauvet, Synth. Met. **121**, 1215 (2001).

[4] E. Kymakis, I. Alexandrou, and G. A. J. Amaratunga, Synth. Met. **127**, 59 (2002).

[5] H. Ago, K. Petritsch, M. S.P. Shafer, D. S. Ginger, A. H. Windle, and R. H. Friend, Adv. Mater. (Weinheim, Ger.) **11**, 1281 (1999).

[6] H. Ago, M. S.P. Shafer, D. S. Ginger, A. H. Windle, R. H. Friend, Phys. Rev. B **61**, 2286 (2000).

[7] C. Yang, M. Wohlgenannt, Z. V. Vardeny, W. J. Blau, A. B. Dalton, R. Baughman, and A. A. Zakhidov, Physica B **388**, 366

(2003).
[8] J. Wéry, H. Aarab, S. Lefrant, E. Faulques, E. Mulazzi, and R. Perego, Phys. Rev. B **67**, 115202 (2003).
[9] C. Journet, W. K. Maser, P. Bernier, A. Loiseau, M. Lamy de la Chapelle, S. Lefrant, P. Deniard, R. Lee, and J. E. Fischer, Nature (London) **388**, 756 (1997).
[10] J. D. Stenger-Smith, R. W. Lenz, and G. Wegner, Polymer **30**, 1048 (1989).
[11] T. Guo, P. Nikolaev, A. G. Rinzler, D. Tomanek, D. T. Colbert, and R. E. Smalley, J. Phys. Chem. **99**, 10694 (1995).
[12] H. Aarab, M. Baitoul, J. Wery, S. Lefrant, E. Faulques, M. Hamedoun (unpublished).
[13] Y. B. Moon, S. D. D. V. Rughooputh, A. J. Heeger, A. O Patil, and F. Wudl, Synth. Met. **29**, E79 (1989).
[14] J. Wéry, B. Dulieu, M. Baitoul, P. Paniez, G. Froyer, and S. Lefrant, Synth. Met. **101**, 194 (1999).
[15] S. Kirkpatrick, Rev. Mod. Phys. **45**, 574 (1973).
[16] R. H. Friend, D. D. C. Bradley, and P. D. Townsend, J. Phys. D **20**, 1367 (1987).
[17] B. Dulieu, J. Wéry, S. Lefrant, and J. Bullot, Phys. Rev. B **57**, 9118 (1998).
[18] E. Mulazzi, A. Ripamonti, J. Wéry, B. Dulieu, and S. Lefrant, Phys. Rev. B **60**, 16 519 (1999).
[19] N. Bendiab, R. Almairac, M. Paillet, and J. L. Sauvajol, Chem. Phys. Lett. **372**, 210 (2003).
[20] S. Lefrant, J. P. Buisson, O. Chauvet, and J. M. Benoit, in *Making Functional Materials with Nanotubes*, edited by P. Nikoleav, P. Bernier, P. Ajayan, and Y. Iwasa, Mater. Res. Soc. Symp. Proc. No. **706** (Material Research Society, Pittsburgh, PA, 2002), p. Z7.2.
[21] Henrard, E. Hernandez, P. Bernier, and A. Rubio, Phys. Rev. B **60**, R8521 (1999).
[22] D. Kahn and J. Yu, Phys. Rev. B **60**, 6535 (1999).
[23] I. Orion, J. P. Buisson, and S. Lefrant, Phys. Rev. B **57**, 7050 (1998).
[24] S. D. M. Brown, P. Corio, A. Marucci, M. S. Dresselhaus, M. A. Pimenta, and K. Kneipp, Phys. Rev. B **61**, R5137 (2000).
[25] J. Wéry, B. Dulieu, J. Bullot, M. Baitoul, P. Deniard, and J. P. Buisson, Polymer **40**, 519 (1999).
[26] J. Yu, N. S. Farm, F. J. Cao, D. Y. Yang, and S. H. Lin, Synth. Met. **66**, 143 (1994).
[27] J. Cornil, D. Beljonne, Z. Schuai, T. W. Hagler, J. Campbell, D. D. C. Bradley, J. L. Brédas, C. W. Spangler, and K. Müller, Chem. Phys. Lett. **247**, 425 (1995).
[28] G. P. Brivio and E. Mulazzi, Phys. Rev. B **30**, 876 (1984).
[29] J. Schreiber, Ph.D. thesis, Nantes University, 2002.
[30] J. P. Buisson, O. Chauvet, S. Lefrant, J. M. Benoit, C. Godon, and C. Stephan, in *Electronic Properties of Molecular Nanostructures*, edited by H. Kuzmany *et al.*, AIP Conf. Proc. No. 591 (AIP, Woodbury, NY, 2001), p. 430.
[31] C. Stéphan, Ph.D. thesis, Nantes University, 2000.
[32] J. J. M. Halls, K. Pichler, R. H. Friend, S. C. Moratti, and A. B. Holmes, Synth. Met. **77**, 277 (1996).
[33] S. V. Frolov, P. A. Lane, M. Ozaki, K. Yoshino, and Z. V. Vardeny, Chem. Phys. Lett. **286**, 21 (1998).